EFFECT OF SPARGER GEOMETRY ON GAS-VOLUME-FRACTION IN BUBBLE-COLUMN FLOWS MEASURED BY GAMMA-DENSITOMETRY TOMOGRAPHY (GDT)

K. A. Shollenberger, D. L. George, and J. R. Torczynski

Engineering Sciences Center
Sandia National Laboratories†
Albuquerque, New Mexico 87185-0834 USA

Key Words: Bubble Column, Gamma-Densitometry Tomography, Gas-Volume Fraction, and Sparger

Prepared for presentation at AIChE 2000 Annual Meeting
Los Angeles, CA, November 12-17, 2000

† Sandia is a multiprogram laboratory operated by Sandia Corporation, a Lockheed Martin Company, for the United States Department of Energy under Contract DE-AC04-94AL85000.

DISCLAIMER

Abstract

Gamma-densitometry tomography (GDT) is applied to study the effect of sparger geometry on the axial development of gas-volume-fraction profiles in a vertical bubble-column flow. Tests are conducted in a cylindrical vessel with an inner diameter of 0.48 m and a height of 3 m using air for the gas phase and lightweight mineral oil (Drakeol 10) for the liquid phase. A cross sparger with interchangeable arms is used to inject gas into the column at a height of 0.33 to 0.36 diameters above the bottom of the column. The superficial gas velocity ranges from 5 to 30 cm/s, and the absolute column pressure ranges from 103 to 517 kPa. Radial distributions of gas volume fraction at eight axial locations from five different sparger geometries are presented. The sparger parameters examined are total open area of the holes, number of holes, hole diameter, and hole orientation. The development length of the gas-volume-fraction profile is found to increase with gas flow rate and column pressure for all sparger geometries tested. A comparison of the results from the five spargers indicates changes in development length of less than one diameter as the number and size of sparger holes are varied. More significant changes in development length, by as much as four diameters at the highest gas velocity and column pressure, are found when varying hole orientation alone. For all spargers tested, average values of gas volume fraction in the fully developed region of the column differ by less than ±0.02 for the same flow conditions.

Introduction

Slurry bubble-column reactors, or SBCRs, are cylindrical vessels in which a reactive gas is bubbled through a catalyst-laden liquid to produce a desired chemical. The distribution of the phases is important because significant spatial variations can induce large-scale, buoyancy-driven motions that can reduce gas residence time in a reactor and thus decrease process efficiency. Because the flow in an SBCR is generally a very complicated turbulent multiphase mixture,

fundamental characterization and modeling of the hydrodynamics remains a formidable task. In particular it is important to understand how operating parameters, such as gas flow rate, column pressure, and sparger (gas injector) design, can change the gas distribution in a bubble column reactor.

To assist in the design and scaleup of SBCRs, Sandia National Laboratories is conducting research on the hydrodynamic behavior of vertical multiphase flows. Research at Sandia currently involves the development and application of nonintrusive diagnostic methods on both the laboratory and industrial scales. The eventual goal of this work is to use these diagnostics to determine the phase distributions in SBCR vessels at conditions similar to those in industry. Such information can be used to improve indirect coal liquefaction and other industrial processes. The specific objective of this paper is to provide an assessment of how sparger design affects the gas volume fraction distribution in the developing region of an SBCR vessel over a broad range of gas flow rates and column pressures. The sparger parameters studied include porosity (ratio of sparger total hole area to column area), the number and size of holes for a fixed porosity, and the hole orientation. Gamma-densitometry tomography (GDT) is applied to measure the gas distributions in the gas-liquid flows. Results are presented that will be used as detailed data sets for multiphase model development.

Gamma-Densitometry Tomography (GDT) System

The gamma-densitometry tomography (GDT) system developed for studies of industrial-scale multiphase flows is shown in Figure 1 (Torczynski et al., 1996; Shollenberger et al., 1997). The system consists of a 5-curie ^{137}Cs gamma source, a sodium-iodide detector system, a traverse, and hardware and software for data acquisition and system control. The horizontal

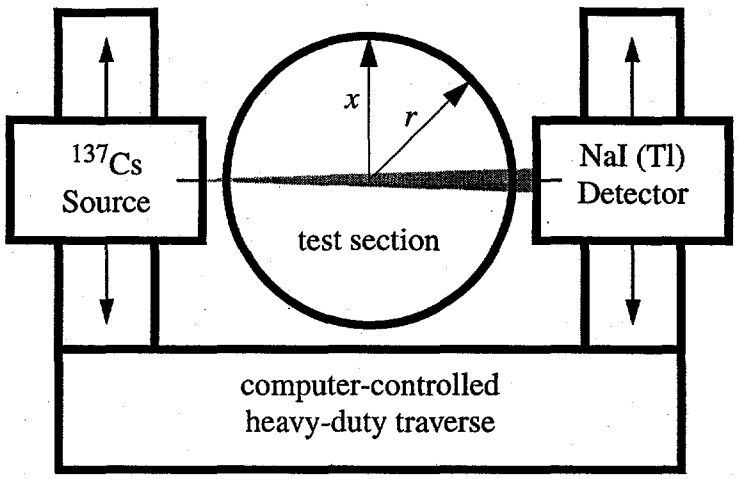

Figure 1. Schematic of gamma-densitometry tomography (GDT) system in the horizontal plane.

traverse is used to position the source and detector, on opposite sides of the column, at locations ranging from one side of the column to the other. Gamma-ray intensity is measured along parallel beam paths through the column and then translated into gas volume fraction averaged along each path using measurements of the intensities with the vessel empty and full of liquid. A curve fit to these data points is then found using a polynomial in even powers of x to any chosen order. Finally, the Abel transform (Vest, 1985) is used to convert the path-averaged gas-volume-fraction profile in x into a radial gas-volume-fraction profile (a polynomial in even powers of r) in the circular domain. The Abel transform uses the assumption of an axisymmetric phase distribution, an assumption that is valid for many vertical gas-liquid flows when averaged over long time scales. For the flows considered here, GDT measurements across a single horizontal plane require approximately 15 minutes; hence all measurements are inherently time averaged. The horizontal traverse is attached to a 3-m vertical traverse to allow GDT scans at axial locations ranging from approximately 1 diameter above the bottom of the column to the top of the column. Together, the horizontal and vertical traverses allow the effects of sparger parameters on the development of the radial and axial gas distributions in the bubble column to be determined.

Experimental Setup

The sparger study is conducted in a slurry bubble-column reactor (SBCR) testbed installed at Sandia for hydrodynamic experiments at industrially relevant conditions. The SBCR, shown in Figure 2, has an inner diameter of 0.483 m and an inner height of 3.15 m. The column is rated for headspace pressures (P_C) up to 689 kPa gauge and temperatures up to 200 °C. A total of 24 ports, positioned 0.457 m apart at six levels along the column, are used for viewing the flow or as instrumentation ports. Currently, the column is instrumented with pressure diagnostics at all levels and thermocouples at the column wall. Drakeol™ 10, a light mineral oil with a viscosity of 35 cP and a specific gravity of 0.85 at 20 °C, is used as the liquid phase in these experiments in batch mode (i.e. with no net liquid flow). Dry air is introduced near the bottom of the column through an inerchangeable cross sparger (air injector) from a high-pressure air supply tank. Air volumetric

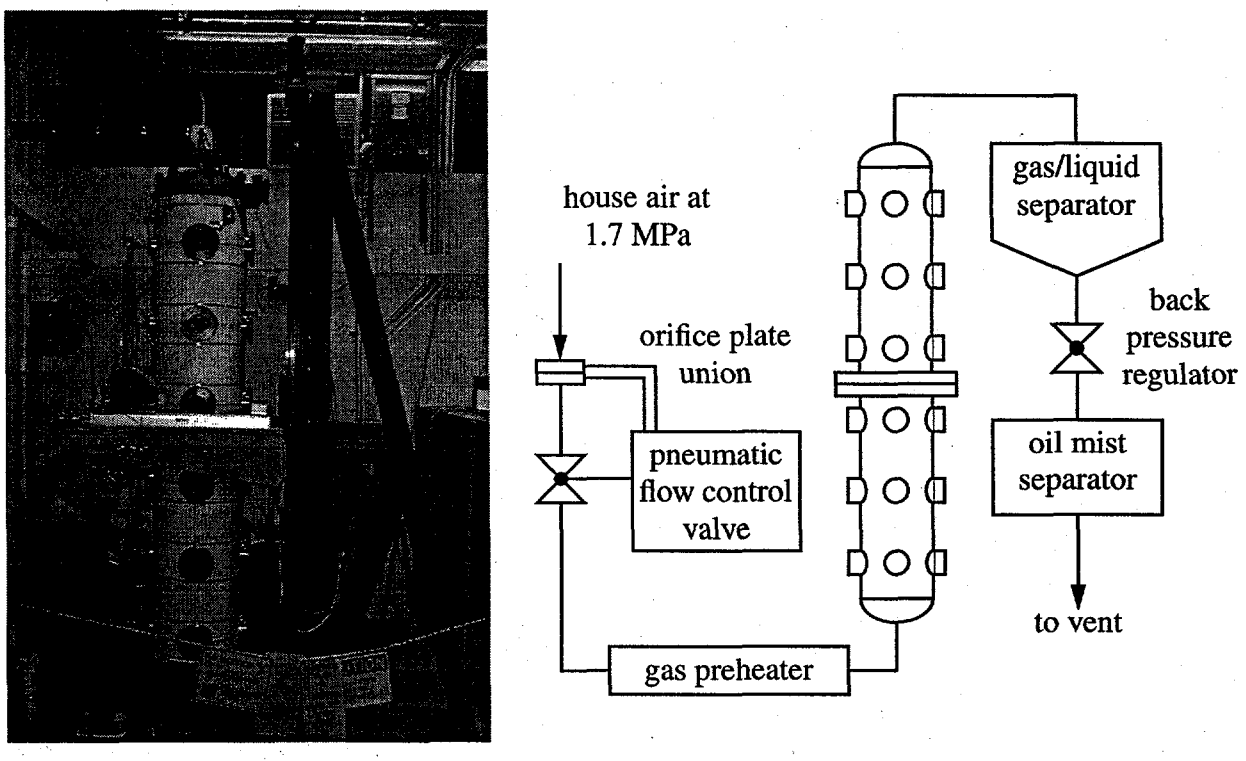

Figure 2. Picture and schematic of the slurry bubble-column reactor (SBCR). In the picture the vertical traverse is to the right of the column; the source and its horizontal traverse are in front.

flow rates up to 3300 L/min, corresponding to superficial gas velocities (U_G, the average vertical velocity the gas would have if it flowed through the column alone) up to 30 cm/s, produce churn-turbulent flow conditions in the column.

Five cross-shaped spargers are used in the SBCR for this study; Table 1 provides a list of each of their geometric parameters. All spargers are made of stainless steel, have identical arms of 1.59-cm ID stainless tubing, and have an arm span of 45.4 cm. One-quarter of the total number of holes for each sparger resides on each of the four arms, and the holes are spaced evenly on each arm over a distance of 15.2 cm. Sparger A has a porosity of 0.05%, and the remaining spargers have a porosity of 0.10%, where porosity is defined as the ratio of the sparger total hole area to the column area. A transition to sonic flow through the sparger holes occurs at a superficial gas velocity in the column of 20 cm/s for 0.05% porosity and at 40 cm/s at 0.10% porosity. The ratio of the hole area of each sparger to the cross-sectional area of all four pipe arms is 12% for 0.05% porosity and 24% for 0.10% porosity. Thus, there is a reasonable restriction across each sparger that should help to ensure that all sparger holes are activated. Spargers A, B, and D are mounted in the vessel such that the holes face upwards and are located $z = 0.176$ m above the vessel bottom, at a nondimensionalized height $z/D = 0.36$. Spargers E and F are produced by rotating the arms of Sparger B so that the holes face downwards and sideways, respectively. For these cases the

Table 1. Specifications for the cross spargers used in this study.

Sparger	Porosity	Number of Holes	Hole Dia. (mm)	Hole Orientation
A	0.05%	120	1.0	upwards
B	0.1%	96	1.55	upwards
D	0.1%	4	7.60	upwards
E	0.1%	96	1.55	downwards
F	0.1%	96	1.55	sideways

holes are located at elevations of $z = 0.157$ and 0.167 m, or $z/D = 0.33$ and 0.35, above the vessel bottom, respectively.

For each sparger configuration, the column is initially filled with liquid to a depth of $z = 1.93$ m ($z/D = 4.0$). A matrix of up to six superficial gas velocities ($U_G = 5$, 10, 15, 20, 25, and 30 cm/s) and five headspace pressures ($P_C = 0.10$, 0.21, 0.31, 0.41, and 0.52 MPa) is then applied. The superficial gas velocity is calculated from the pressure drop across an orifice plate, the absolute column pressure, the orifice temperature, and the column temperature. At each set of conditions, horizontal planes are scanned using GDT to determine the gas-volume-fraction radial profiles. GDT measurements are taken at 11 horizontal locations, each for a 60-s duration, and at 8 vertical locations, $z = 0.546$ m to 2.146 m ($z/D = 1.1$ to 4.4) in steps of 0.229 m ($z/D = 0.47$).

Results and Discussion

As stated above, GDT data are acquired at 11 horizontal positions for each reconstructed radial gas volume fraction profile. Figure 3 shows these data points converted to ray-averaged gas volume fractions (in x), a curve fit to the data, and the reconstructed radial gas-volume-fraction profile (in r) at 8 elevations for Sparger A. The data demonstrate that the left-right symmetry is very consistent, justifying the assumption of a time-averaged axisymmetric flow. A fourth-order polynomial in even powers of x is used in all of these plots to curve fit the data with a maximum difference in gas volume fraction from the data of ±0.017. A higher-order curve fit does not reduce this deviation significantly, so fourth-order polynomials are used for all the data presented. Finally, note that the actual gas-volume-fraction value near the centerline is generally much

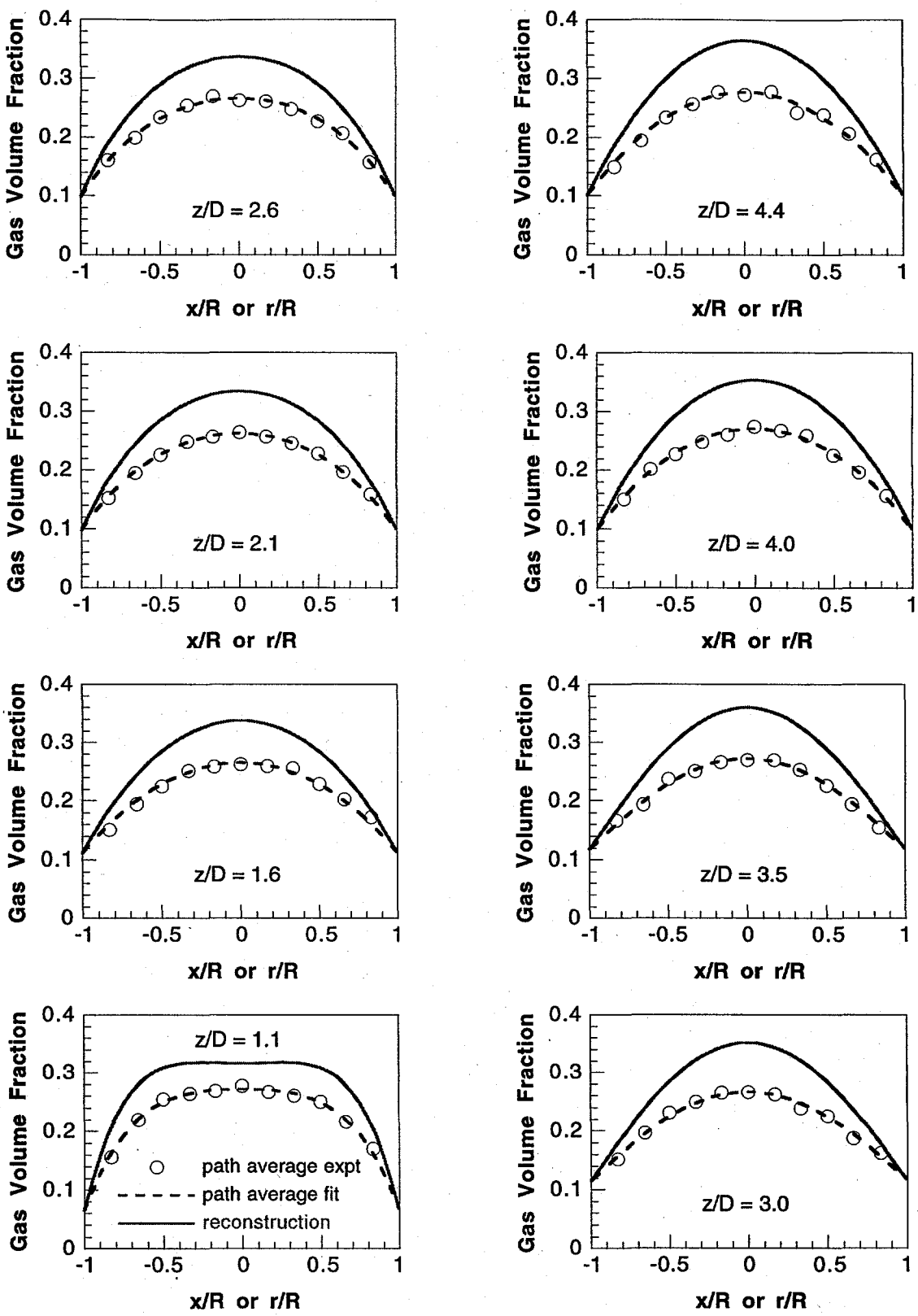

Figure 3. Gas volume fraction: path averaged data points, path average curve fit, and radial reconstruction for Sparger A at 8 axial locations, 20 cm/s, and 0.21 MPa. Legend in bottom left plot.

higher than the ray-averaged value, demonstrating the importance of performing the reconstruction to determine the actual radial distribution.

In order to test the reproducibility of the results, several experiments for Sparger A were repeated before and after all the other runs performed with Spargers B, D, E, and F. Figure 4 shows the radial gas-volume-fraction profiles, $\varepsilon_G(r)$, for Sparger A as a function of z/D with $U_G = 20$ cm/s and $P_C = 0.21$ MPa. The two runs taken at the beginning of this test series are labeled Test 1, and the run labeled Test 2 was acquired at the end. All of the profiles for these cases agree very well, with gas volume fractions agreeing to within ±0.01, except at $z/D = 3.0$. Cross-sectionally averaging the data in Figure 4 and the data from three additional cases indicates measured gas volume fraction variations of ±0.006. These variations are comparable to the experimental uncertainty expected for the GDT system.

Some of the results for Sparger A are presented before comparing different spargers in order to describe some of the general characteristics found for all spargers tested. Figure 5 shows $\varepsilon_G(r)$ as a function of U_G and z/D at $P_C = 0.21$ MPa. At the lowest elevation, $z/D = 1.1$, the profiles at all the given flow rates are flat in the middle and drop off rapidly near the walls. The width of the flat region increases slightly as U_G is increased. By the next elevation, $z/D = 1.6$, and for the remainder of the column, the profiles become more rounded at the center. Figure 6 shows $\varepsilon_G(r)$ as a function of P_C and z/D at $U_G = 20$ cm/s. Again, the profiles shift from flat to rounded at the middle between the bottom two elevations, and the width of the flat region increases slightly as P_C is increased. Comparing Figures 5 and 6, it is seen that gas volume fraction is more sensitive to changes in superficial gas velocity than column pressure. In addition, it is found that as the superficial gas flow rate is increased, the gas-volume-fraction profiles increase

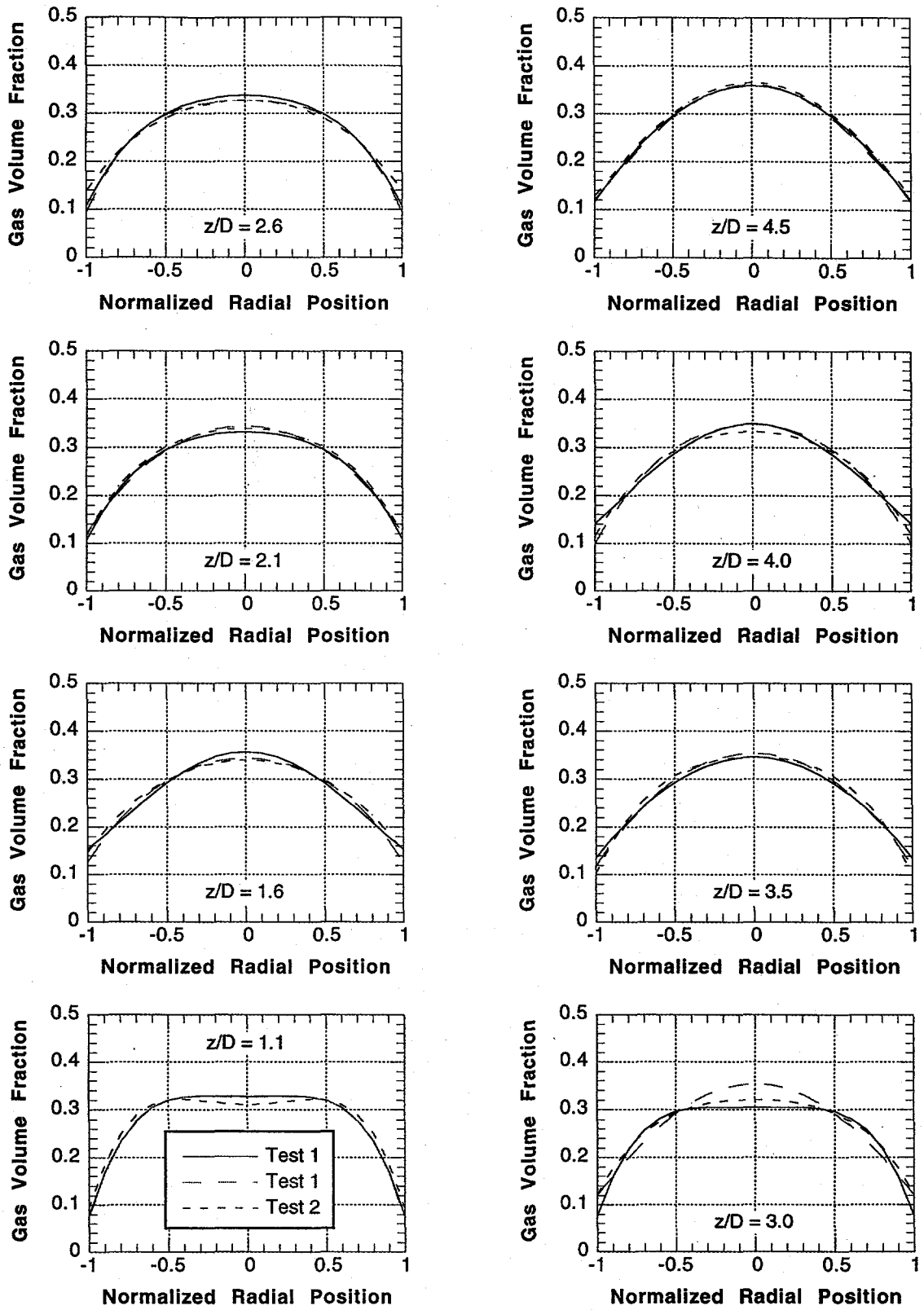

Figure 4. Comparison of gas-volume-fraction profiles versus normalized axial position (*z/D*) for Sparger A at 20 cm/s and 0.21 MPa. Legend in bottom left plot.

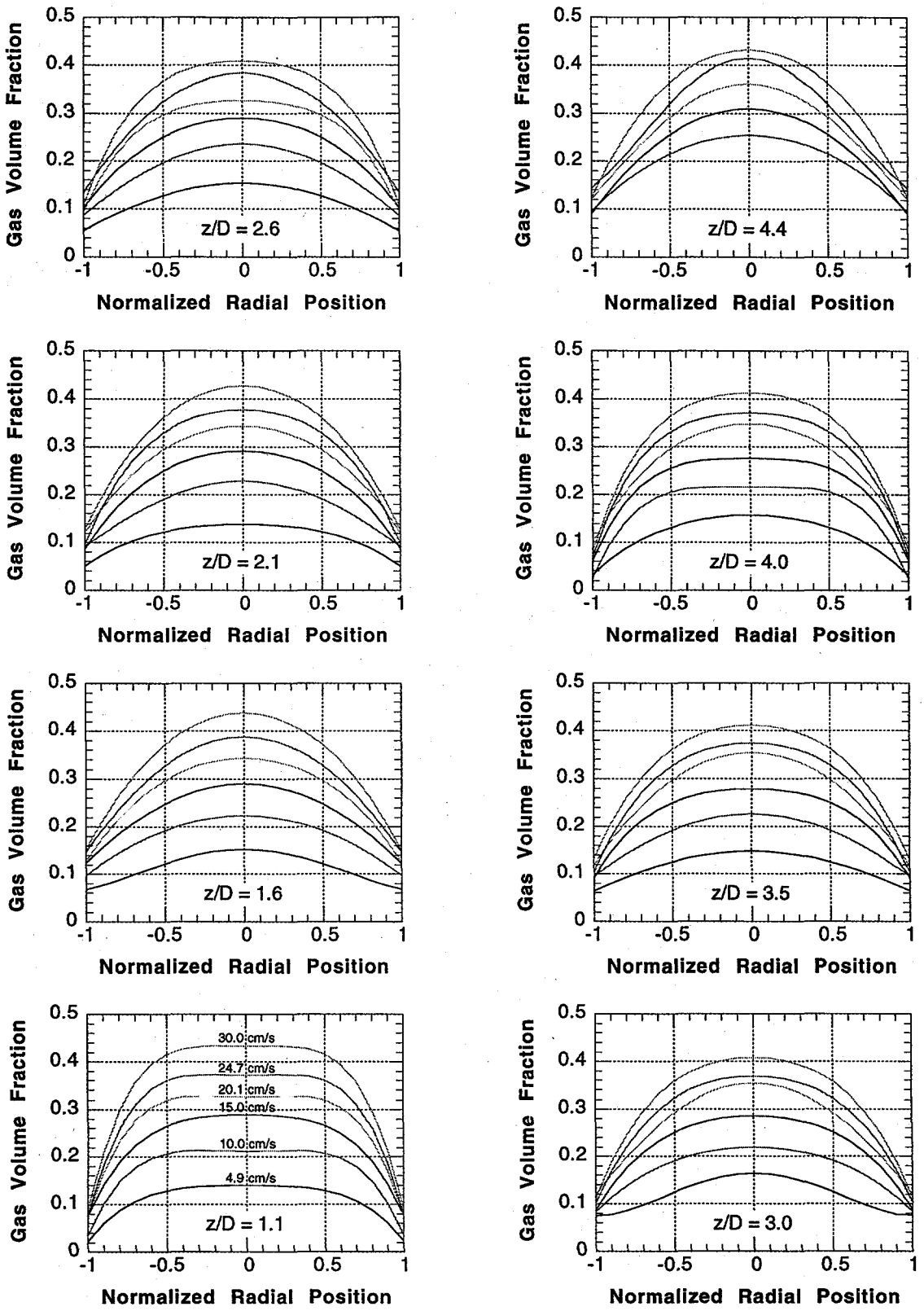

Figure 5. Gas-volume-fraction profiles versus normalized axial position (z/D) and superficial gas velocity for Sparger A at 0.21 MPa. Legend in bottom left plot.

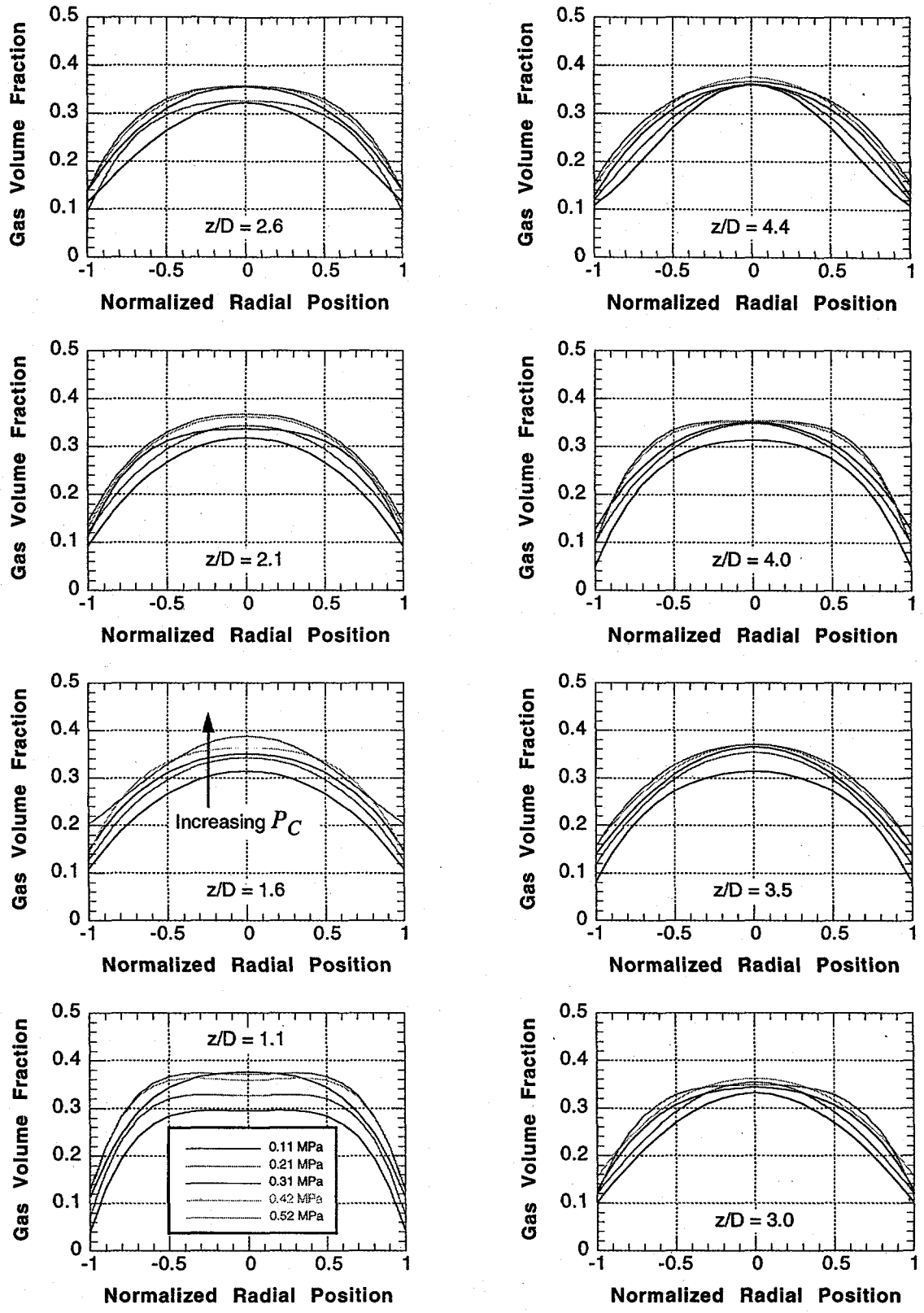

Figure 6. Gas-volume-fraction profiles versus normalized axial position (z/D) and column pressure for Sparger A at 20 cm/s. Legend in bottom left plot.

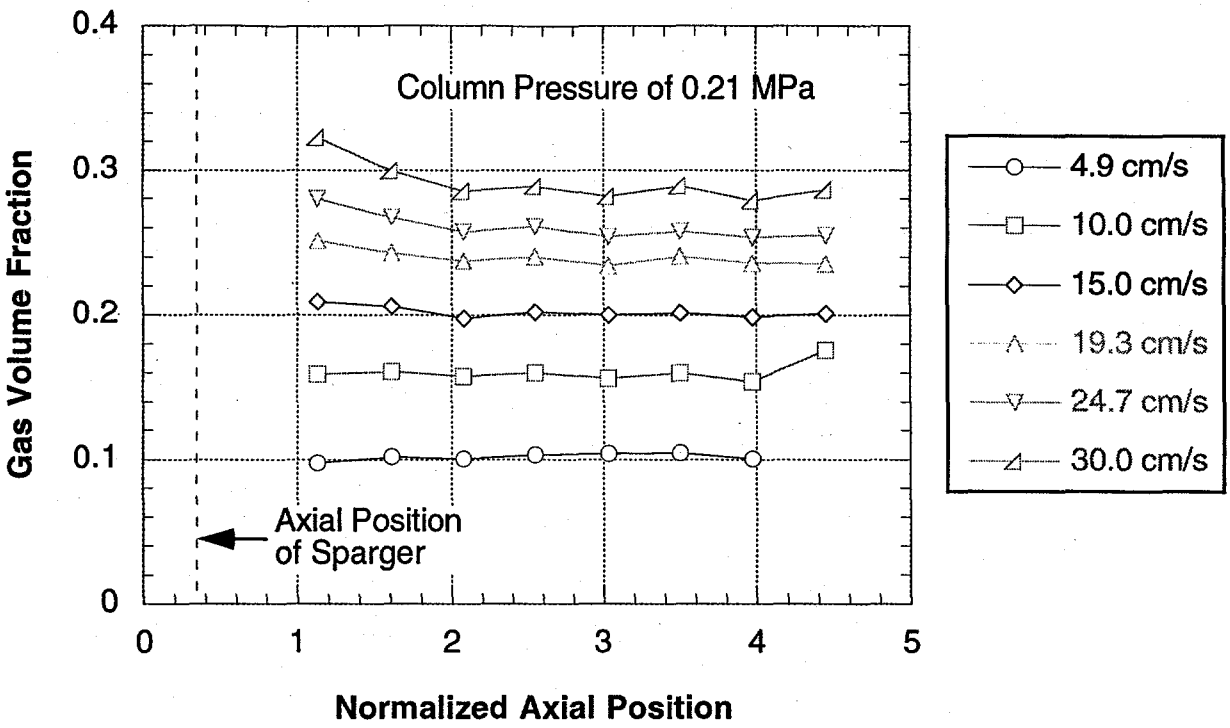

Figure 7. Cross-sectionally averaged gas volume fraction as a function of nondimensionalized axial position and superficial gas velocity for Sparger A at 0.21 MPa.

preferentially near the centerline. Conversely, as the column pressure is increased, the gas-volume-fraction profiles generally shift uniformly upward across the column diameter.

Cross-sectionally averaging the data in Figures 5 and 6 produces Figures 7 and 8, respectively, which show the gas-volume-fraction axial profiles or changes in gas volume fraction as axial position goes from $z = 0$ (the bottom of the vessel) upwards. As noted above from the profile plots, gas volume fraction can readily be seen to increase with both U_G and P_C. For these plots, it is expected that if the gas-volume-fraction profile is fully developed (i.e. no longer changing as the axial position changes) then the cross-sectionally averaged gas volume fraction should be constant with increasing axial position. Figure 7 shows that the flow is fully developed for $z/D > 1.1$ at $U_G \leq 10$ cm/s, but the development length for the flow increases to about $z/D = 2$ as U_G increases to 30 cm/s. Similarly, Figure 8 shows that the flow is fully developed

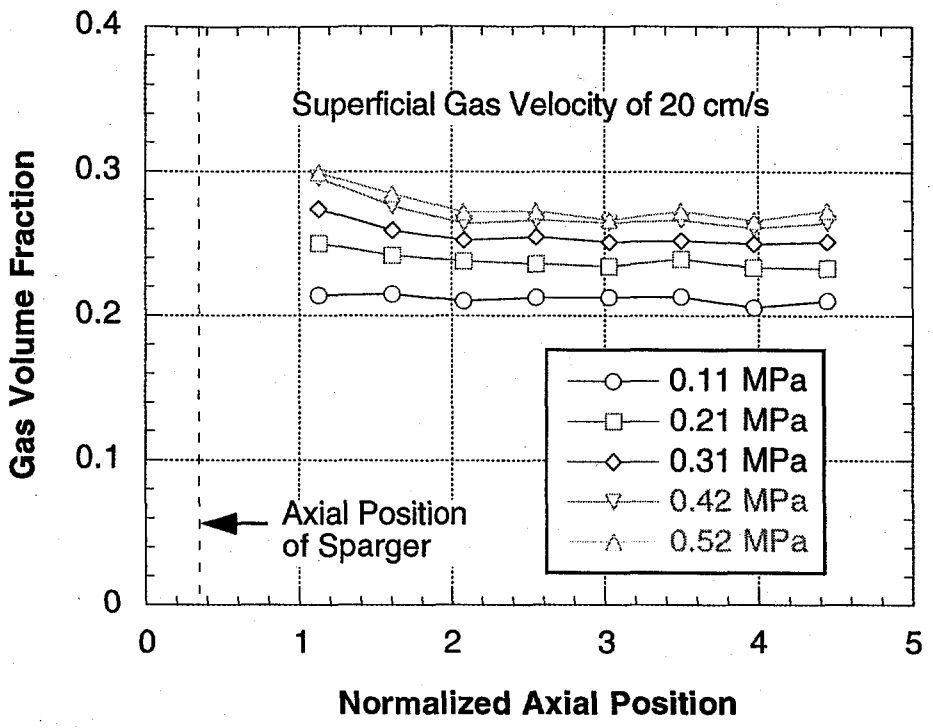

Figure 8. Cross-sectionally averaged gas volume fraction as a function of nondimensionalized axial position and column pressure for Sparger A at 20 cm/s.

for $z/D > 1.1$ at $P_C \leq 0.1$ MPa, but the development length again increases to about $z/D = 2$ as P_C increases to 0.52 MPa. Thus, the length of the development region increases as both U_G and P_C increase.

Sparger Porosity

The first sparger parameter considered is porosity, which is defined as the ratio of the sparger total hole area to the column area. As shown in Table 1, the porosity of Sparger B is twice that of Sparger A. The number and size of holes also change, but both spargers are similar in that they have very many small holes. Figure 9 shows $\varepsilon_G(r)$ as a function of U_G and z/D at $P_C = 0.21$ MPa for Sparger B. Comparing these profiles with those shown for Sparger A in Figure 5, it is found that the gas-volume-fraction profiles at $z/D = 1.1$ change from being flat near the centerline to having an annular maximum at $r/D = 0.6$ as the porosity is increased. It is

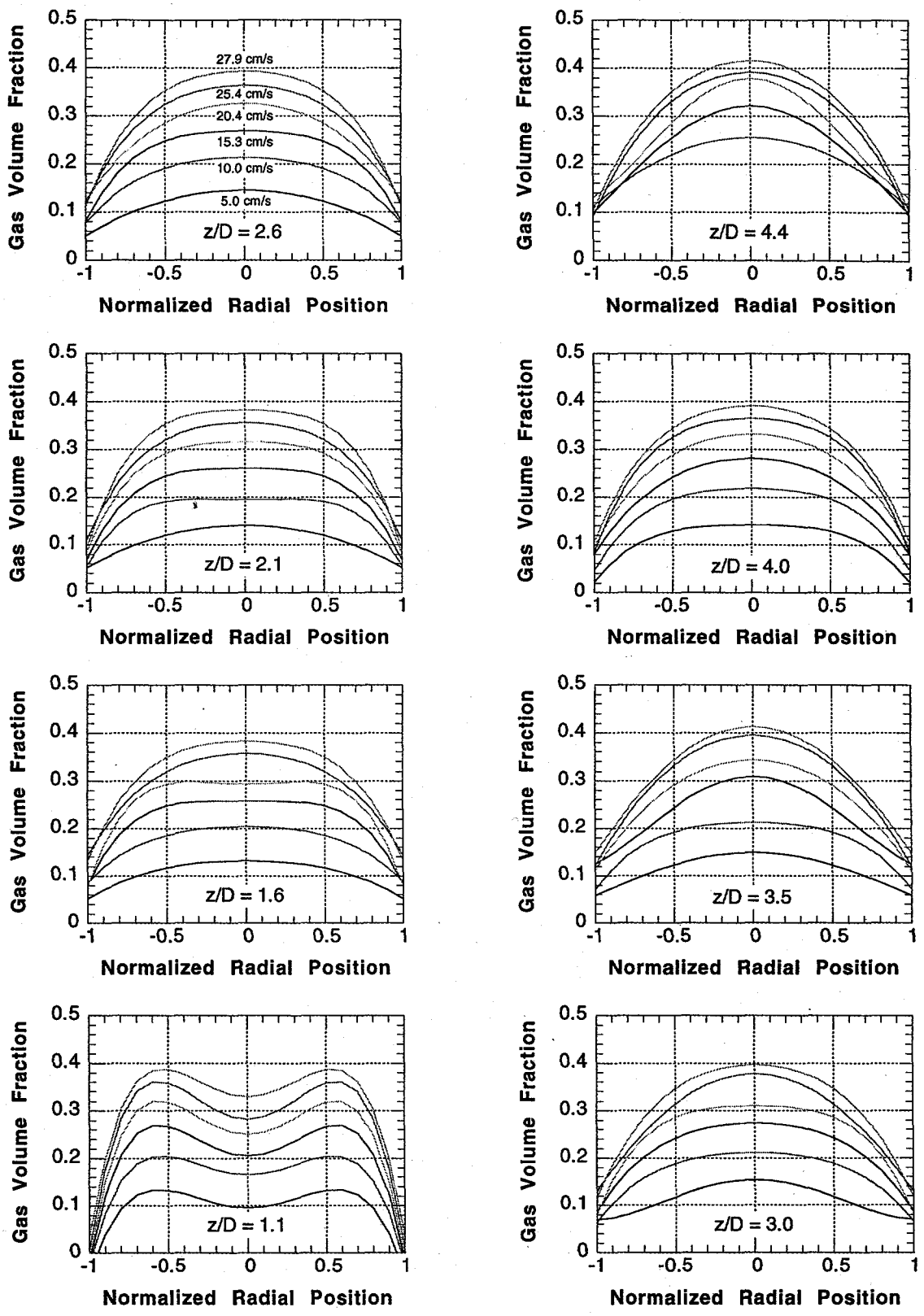

Figure 9. Gas-volume-fraction profiles versus normalized axial position (z/D) and superficial gas velocity for Sparger B at 0.21 MPa. Legend in top left plot.

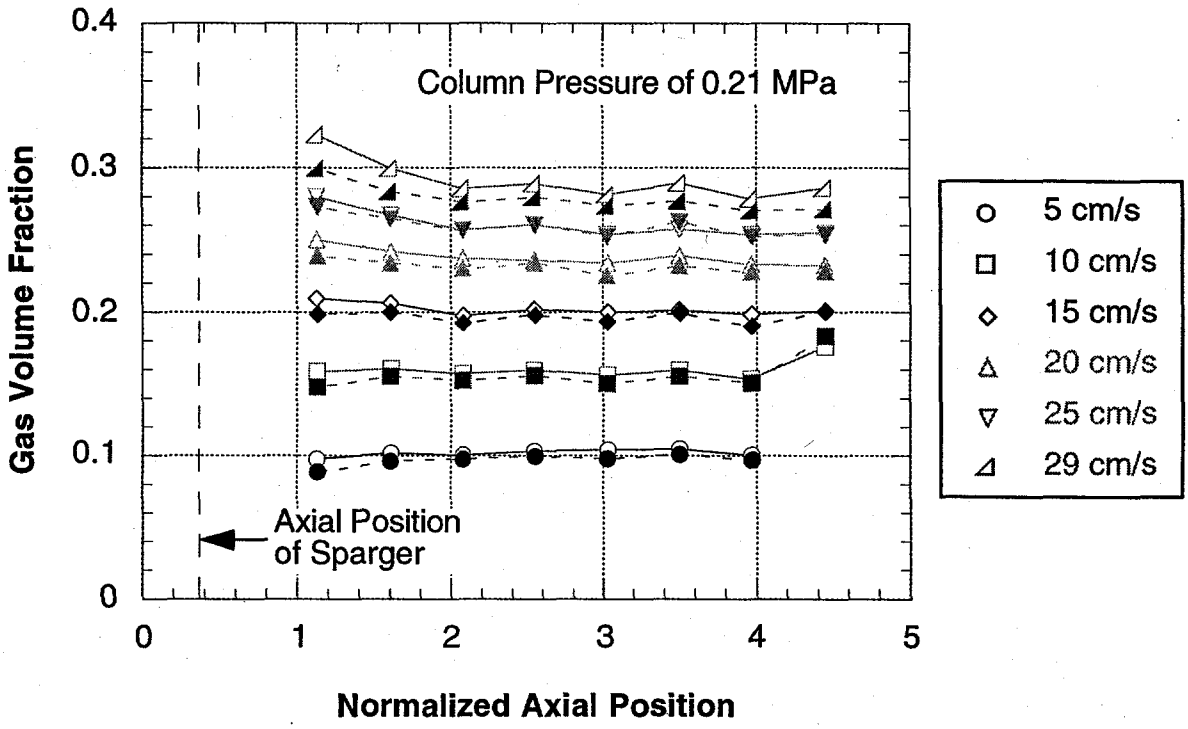

Figure 10. Cross-sectionally averaged gas volume fraction as a function of nondimensionalized axial position and superficial gas velocity for Sparger A (open symbols, solid lines) and Sparger B (closed symbols, dashed lines) at 0.21 MPa.

conjectured that these changes in profile shape are caused by the decrease in momentum of the gas jets for the higher-porosity sparger, resulting in a lower rate of mixing near the sparger and larger nonuniformity. By the next elevation, however, most of the differences in the profile shapes have disappeared, and by the third elevation the profiles for both porosities are very similar. Figure 10 shows the cross-sectionally averaged gas-volume-fraction values for Spargers A and B, which correspond to the profiles in Figures 5 and 9, respectively. This figure shows that even though the radial profiles in the region near the sparger are significantly changed by the porosity, the development lengths are almost the same.

Number and Size of Sparger Holes with Porosity Constant

Spargers B and D were used to compare the effect of the number and size of sparger holes. In these spargers, porosity is held fixed at 0.10% while the number of holes is decreased from 96

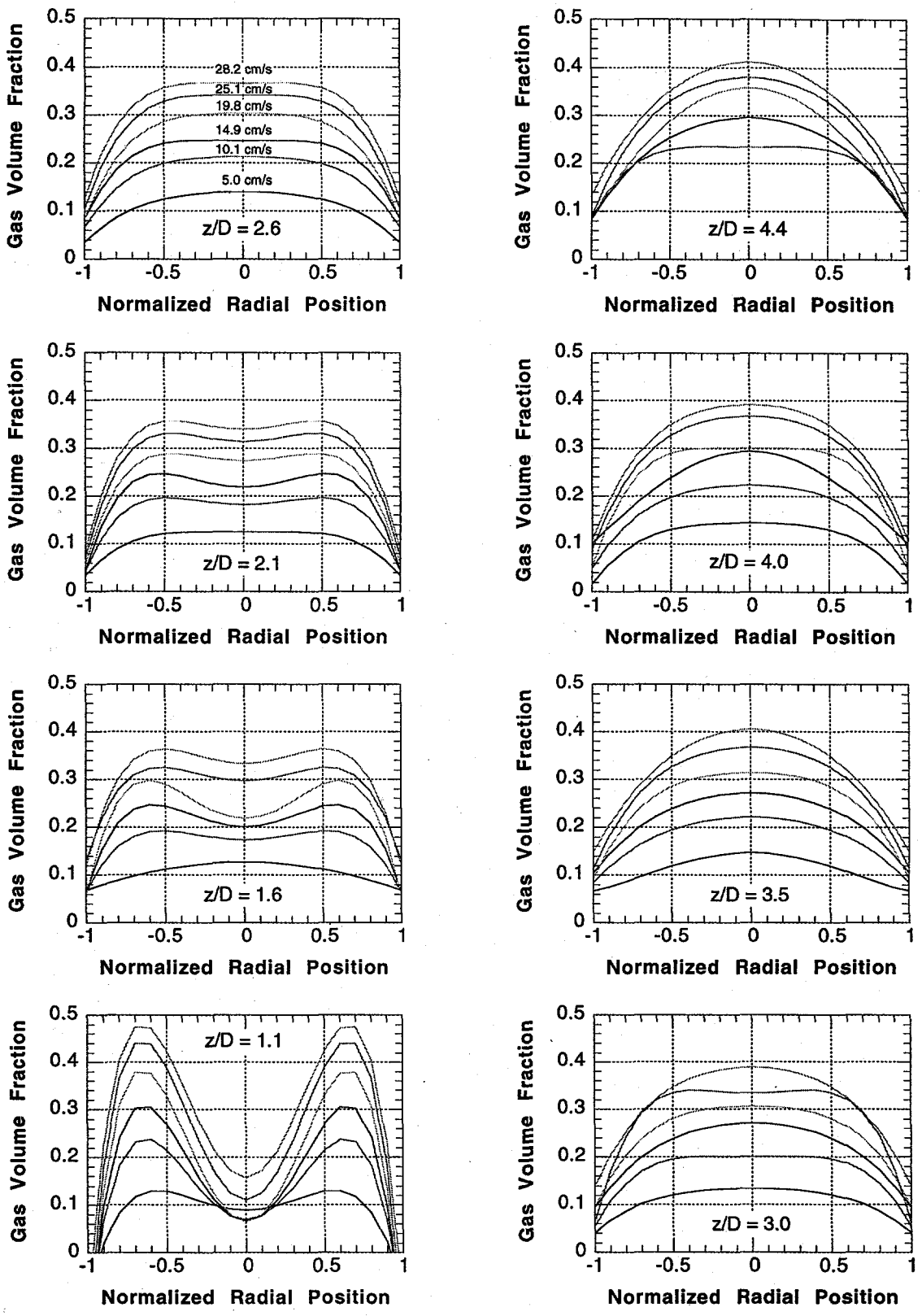

Figure 11. Gas-volume-fraction profiles versus normalized axial position (z/D) and superficial gas velocity for Sparger D at 0.21 MPa. Legend in top left plot.

to 4, requiring an increase in hole size from 1.55 mm in Sparger B to 7.60 mm in Sparger D (see Table 1). Figure 11 shows $\varepsilon_G(r)$ as a function of U_G and z/D at $P_C = 0.21$ MPa for Sparger D. Comparing these profiles with those shown for Sparger B in Figure 9, it is found that the maxima in the gas-volume-fraction profiles at $z/D = 1.1$ are higher in magnitude for Sparger D, which has only 4 holes. The increase in the peak is probably caused by the much coarser spacing of the holes. By the next elevation, however, most of the differences in the profile shapes have once again disappeared, and by the fifth elevation, $z/D = 3.0$, the profiles for each porosity are very similar. Figure 12 shows the cross-sectionally averaged gas-volume-fraction values for Spargers B and D. This figure shows that even though the radial profiles in the region above the sparger are significantly changed by the number of holes, the development lengths are about the same.

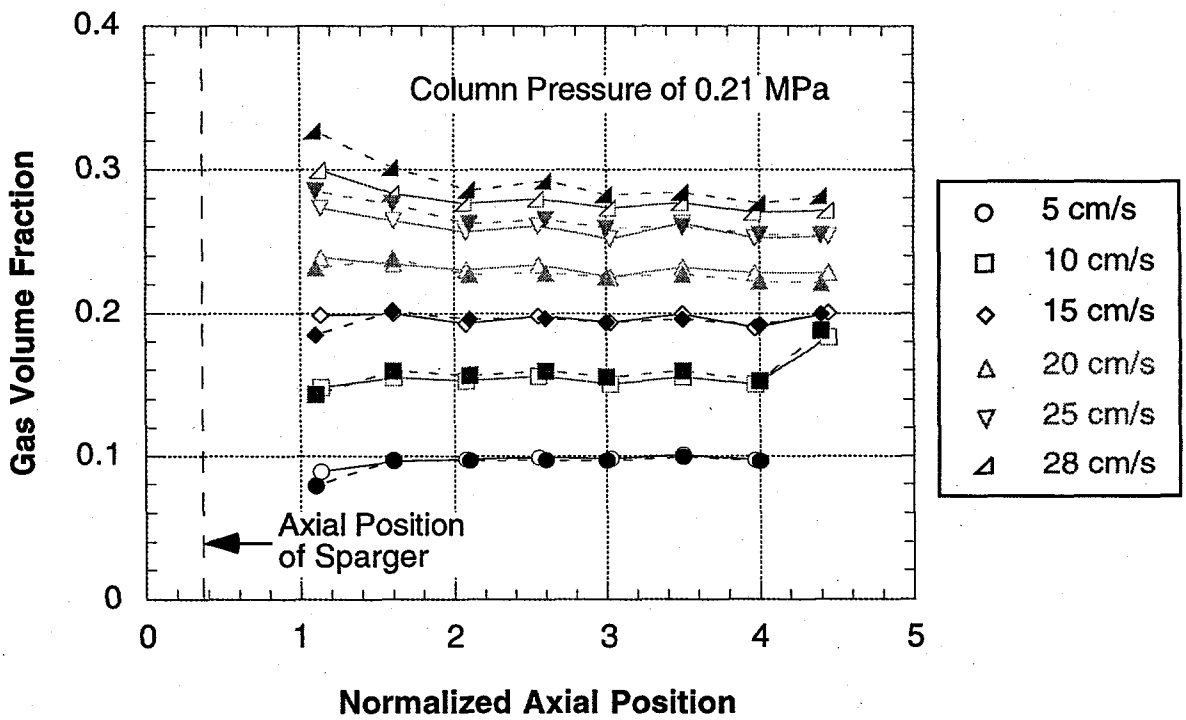

Figure 12. Cross-sectionally averaged gas volume fraction as a function of nondimensionalized axial position and superficial gas velocity for Sparger B (open symbols, solid lines) and Sparger D (closed symbols, dashed lines) at 0.21 MPa.

Sparger Hole Orientation

The final sparger parameter examined is hole orientation, which is changed by rotating the arms of Sparger B. The holes are pointing downwards for Sparger E and sideways in the same azimuthal direction for Sparger F (see Table 1). Figures 13 and 14 show $\varepsilon_G(r)$ as a function of U_G and z/D at $P_C = 0.21$ MPa for Spargers E and F, respectively. Comparing Figure 13 to the profiles for Sparger B shown in Figure 9, it is found that the developing region for the profiles has become less than 1 diameter long for the downward-facing holes. By contrast, the profiles for the sideways-facing holes have a shape that is significantly more pointed than those for the other two hole orientations. Furthermore, these pointed profiles persist through most of the column.

Figures 15 and 16 show radially averaged values for the profiles in Figures 13 and 14, respectively. The data in Figures 15 and 16 can be compared to those presented in Figure 10 for Sparger B, which shows a slight decrease in cross-sectionally averaged gas volume fraction with increasing axial location. Comparing Figures 10 and 15, it is found that the axial profiles for the downwards-facing holes are now constant for all the flow conditions plotted. This agrees with the profile data for Sparger E, which did not change with axial location for the downwards-facing holes. By contrast, the axial profiles for the sideways-facing holes shown in Figure 16 increase with distance along the column and appear to approach a fully developed condition between 2 and 3 diameters for the higher-velocity flow conditions. Note that for all three sparger orientations at low gas velocities, the effect of hole orientation on average gas volume fraction is small. At higher gas velocities, the cross-sectionally averaged gas volume fraction is constant with axial location for downwards-facing holes, decreases for upward-facing holes, and increases for sideways-facing holes. In addition, the development length is 1 to 3 diameters longer for the sideways-

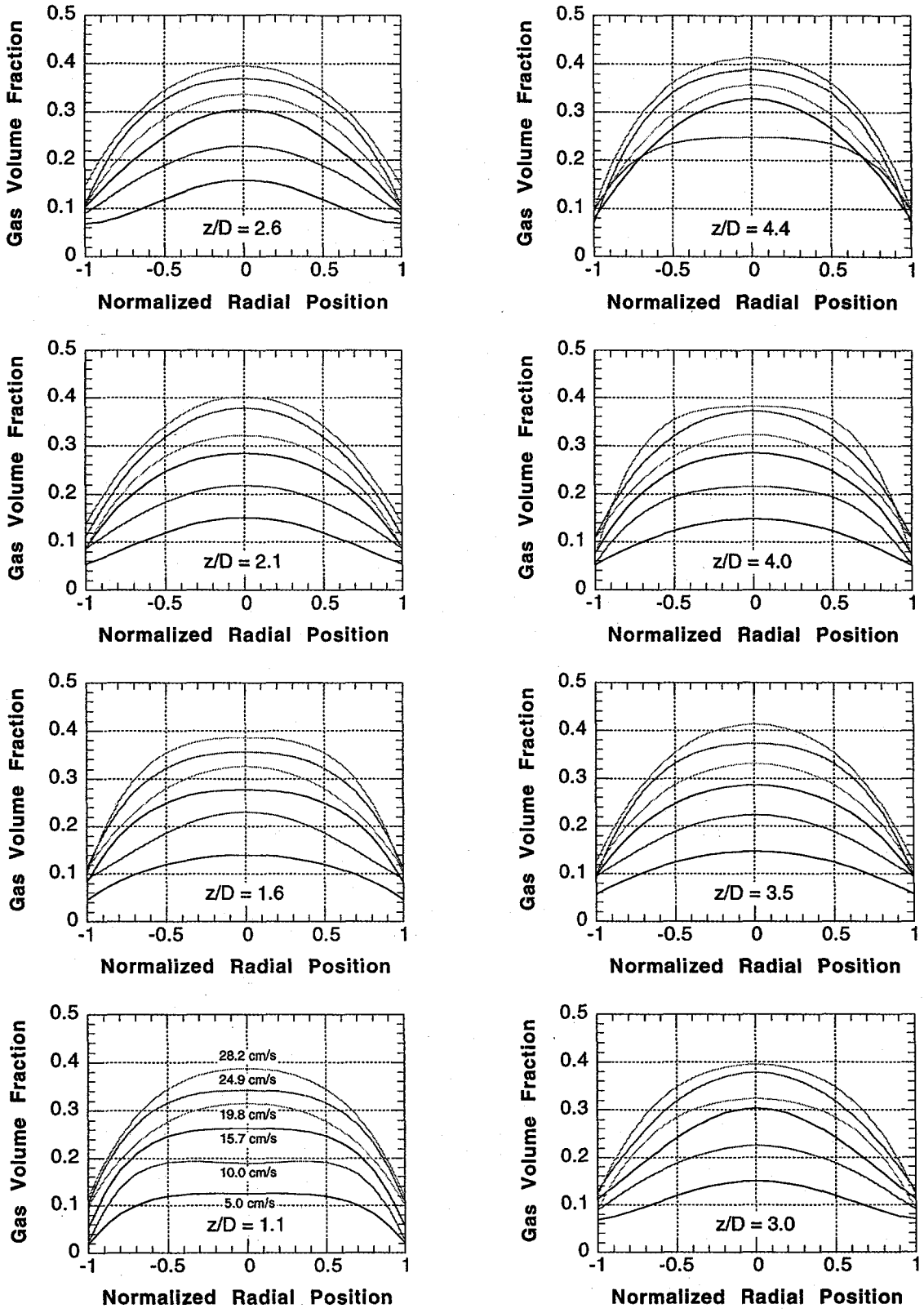

Figure 13. Gas-volume-fraction profiles versus normalized axial position (*z/D*) and superficial gas velocity for Sparger E (downwards holes) at 0.21 MPa. Legend in bottom left plot.

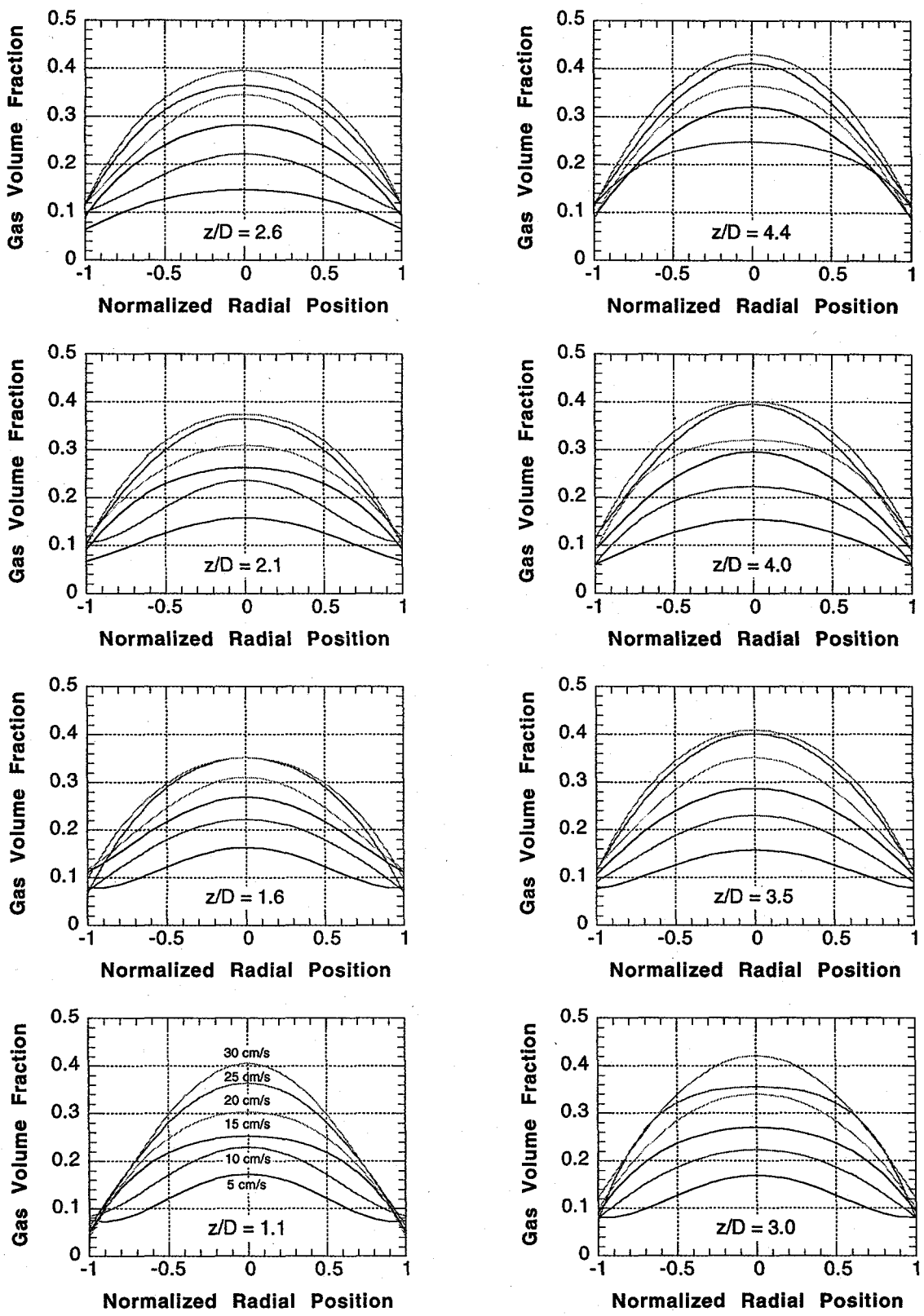

Figure 14. Gas-volume-fraction profiles versus normalized axial position (z/D) and superficial gas velocity for Sparger F (sideways holes) at 0.21 MPa. Legend in bottom left plot.

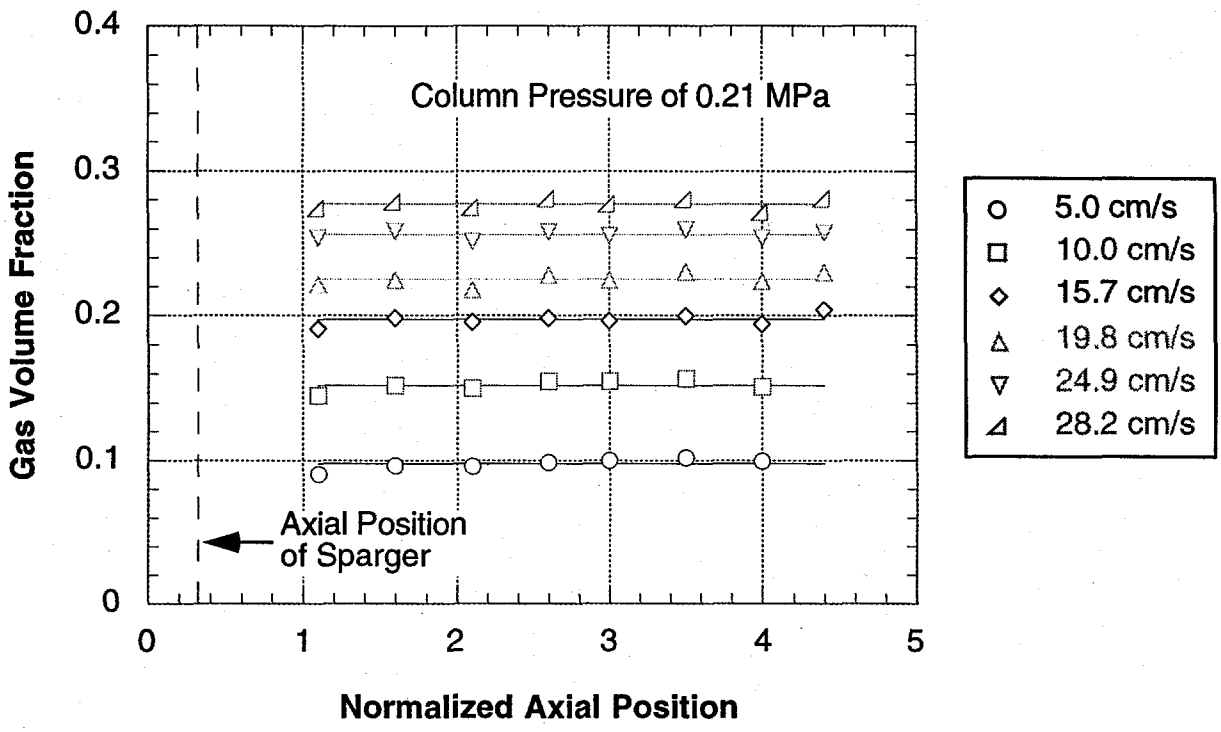

Figure 15. Cross-sectionally averaged gas volume fraction as a function of nondimensionalized axial position and superficial gas velocity for Sparger E (downwards holes) at 0.21 MPa.

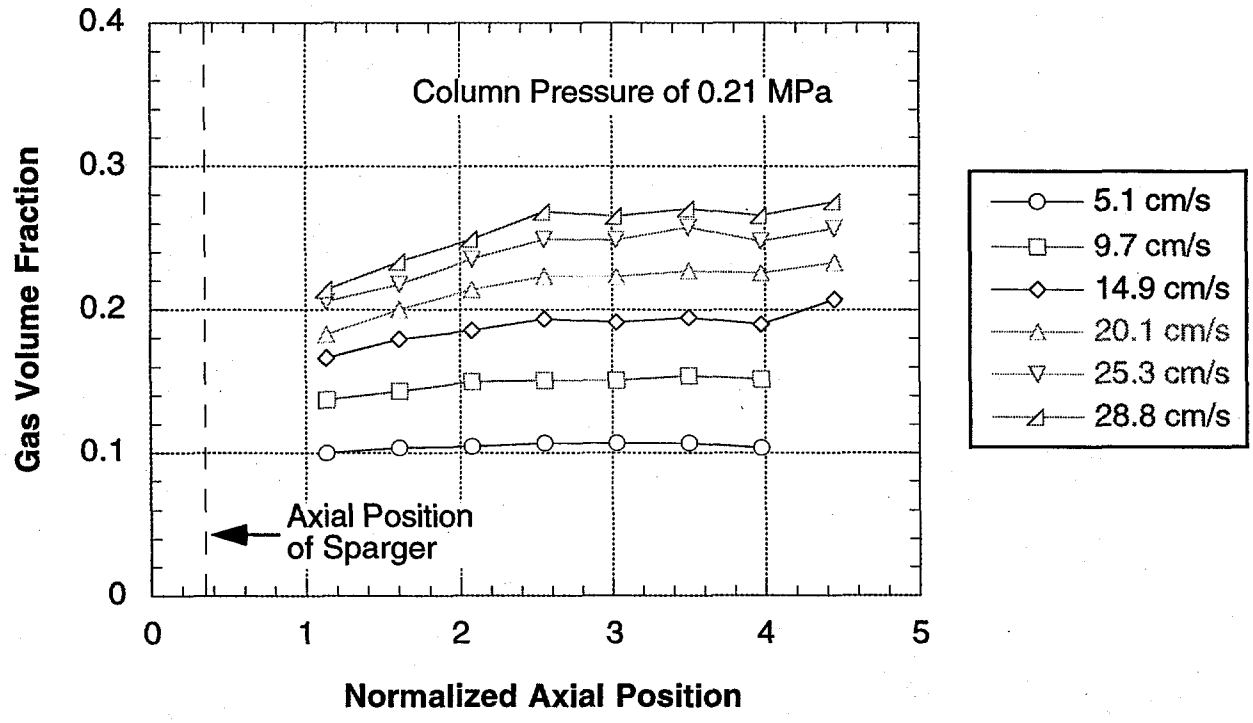

Figure 16. Cross-sectionally averaged gas volume fraction as a function of nondimensionalized axial position and superficial gas velocity for Sparger F (sideways holes) at 0.21 MPa.

facing holes, indicating that the introduction of a radial component in the gas velocity has a significant effect on the development of the gas volume fraction.

Fully Developed Average Gas Volume Fraction

For Spargers A, B, D, E, and F, Figure 17 shows the gas volume fraction averaged over both the cross section and the length of the fully developed region as determined by the profile data. Note that these spargers represent significant differences in porosity, number and size of holes, and hole orientation (see Table 1). The lines drawn in this figure are a strictly empirical correlation:

$$\varepsilon_G = K\,\mathrm{Mo}^{m_1}\left(\frac{\rho_G}{\rho_L}\right)^{m_2}\left(\frac{\mathrm{We}}{\mathrm{Re}}\right)^{m_3} \qquad [1]$$

$$\mathrm{K} = 0.38, m_1 = -0.18, m_2 = 0.18, \text{ and } m_3 = 0.55\,.$$

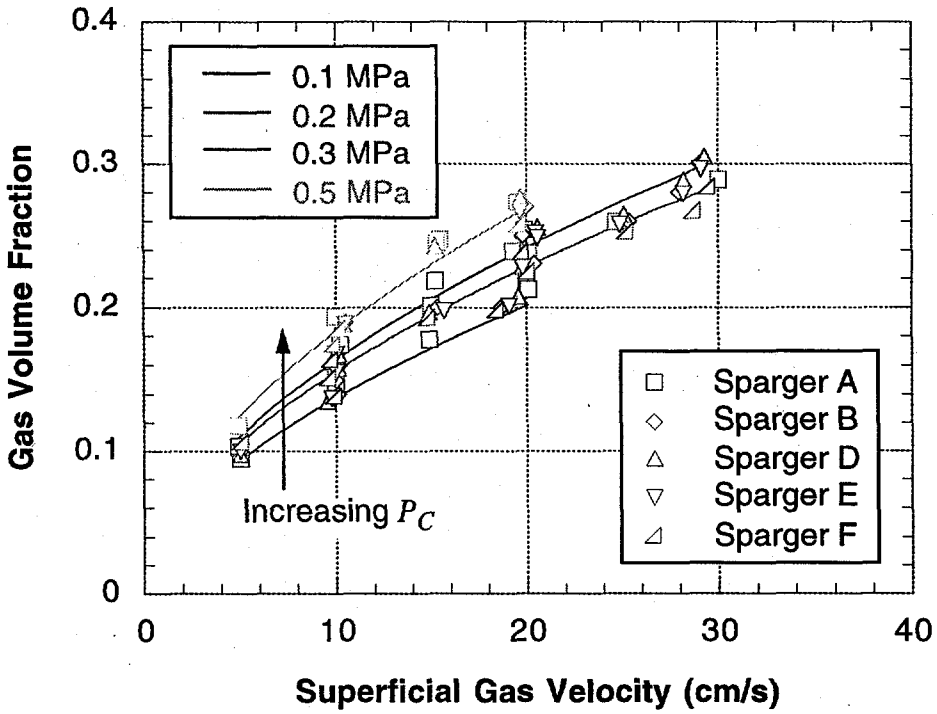

Figure 17. Fully-developed average gas volume fraction as a function of superficial gas velocity and column pressure for all spargers tested.

The Morton number (Mo), the Weber number for the liquid (We_L), and the Reynolds number for the liquid (Re_L) are defined as follows:

$$Mo = \frac{g\,(\rho_L - \rho_G)\,\mu_L^4}{\sigma^3\,\rho_L^2},\ We_L = \frac{U_G^2\,D\,\rho_L}{\sigma},\ \text{and}\ Re_L = \frac{\rho_L\,U_G\,D}{\mu_L}, \qquad [2]$$

where ρ_L is the liquid density, ρ_G is the gas density, σ is the surface tension, μ_L is the liquid viscosity, D is the column diameter, and g is the acceleration due to gravity. Note that the combination of the Weber and Reynolds numbers in the correlation removes the dependence on column diameter in the correlation. The correlation fits all of the average gas volume fraction data presented to within ±0.018. Some of the variation occurs because of the difficulty of sustaining a prescribed pressure over the two-hour duration of an experiment. Also, there are small differences between the data for different spargers, but it is not known at present if these differences are significant.

Conclusions

An experimental study to determine the effect of changing sparger geometry on the development of gas volume fraction profiles has been performed. For all the spargers tested, the entry length increases as both superficial gas velocity and column pressure increase. Increasing the sparger porosity causes the lowest profiles to become more peaked, but this has only a slight effect on entry length. Decreasing the number of sparger holes while keeping the sparger porosity constant again causes the initial profiles to become more peaked, but again this has only a slight effect on entry length. Changing the hole orientation has the largest effect on entry length for the parameters tested. Holes oriented downwards have entry lengths less than 1 diameter. At high gas velocities, holes oriented upwards have an entry length of 1-2 diameters, and holes oriented

sideways have an entry length of 2-3 diameters. All average gas-volume-fraction data for the fully-developed flow can be fit with a non-dimensional correlation to within ±0.018.

Acknowledgments

This work was performed at Sandia National Laboratories. Sandia is a multiprogram laboratory operated by Sandia Corporation, a Lockheed Martin Company, for the United States Department of Energy under Contract DE-AC04-94AL85000. A portion of this work was funded by the National Energy Technology Laboratory under Field Work Proposal FEW-8616. The authors are grateful for technical interactions with B. A. Toseland of Air Products and Chemicals, Inc. The authors would also like to thank C. B. Lafferty and W. C. Ginn for their skilled technical assistance, D. R. Adkins for his early work with the GDT system, and N. B. Jackson for her technical discussions related to catalysis.

References

Shollenberger, K. A., Torczynski, J. R., Adkins, D. R., O'Hern, T. J., and Jackson, N. B. (1997) Gamma-densitometry tomography of gas holdup spatial distribution in industrial-scale bubble columns. *Chem. Eng. Sci.* **52**, 2037-2048.

Torczynski, J. R., Adkins, D. R., Shollenberger, K. A., and O'Hern, T. J. (1996) Application of gamma-densitometry tomography to determine phase spatial variation in two-phase and three-phase bubbly flows. *ASME Cavitation and Multiphase Flow Forum*, FED-Vol. **236**, 503-508.

Vest, C. M. (1985) Tomography for properties of materials that bend rays: a tutorial. *Appl. Opt.* **24**, 4089-4094.